Epilepsia, 53(11):1937–1947, 2012
doi: 10.1111/j.1528-1167.2012.03662.x

FULL-LENGTH ORIGINAL RESEARCH

Altered theta coupling between medial entorhinal cortex and dentate gyrus in temporal lobe epilepsy

*†‡Ulrich P. Froriep, *‡Arvind Kumar, *§¶Delphine Cosandier-Rimélé, #Ute Häussler, *†‡Antje Kilias, *#Carola A. Haas, and *†Ulrich Egert

*Bernstein Center Freiburg, University of Freiburg, Freiburg, Germany; †Biomicrotechnology, Department of Microsystems Engineering, IMTEK, Faculty of Engineering, University of Freiburg, Freiburg, Germany; ‡Neurobiology and Biophysics, Faculty of Biology, University of Freiburg, Freiburg, Germany; §INSERM, UMR 1099, Rennes, France; ¶LTSI, University of Rennes 1, Rennes, France; and #Experimental Epilepsy Research, Department of Neurosurgery, Faculty of Medicine, University of Freiburg, Freiburg, Germany

Summary

Purpose: Temporal lobe epilepsy is often accompanied by neuron loss and rewiring in the hippocampus. We hypothesized that the interaction of subnetworks of the entorhinal–hippocampal loop between epileptic events should show significant signatures of these pathologic changes.

Methods: We combined simultaneous recording of local field potentials in entorhinal cortex (EC) and dentate gyrus (DG) in freely behaving kainate-injected mice with histologic analyses and computational modeling.

Key Findings: In healthy mice, theta band activity was synchronized between EC and DG. In contrast, in epileptic mice, theta activity in the EC was delayed with respect to the DG. A computational neural mass model suggests that hippocampal cell loss imbalances the coupling of subnetworks, introducing the shift.

Significance: We show that pathologic dynamics in epilepsy encompass ongoing activity in the entorhinal-hippocampal loop beyond acute epileptiform activity. This predominantly affects theta band activity, which links this shift in entorhinal-hippocampal interaction to behavioral aspects in epilepsy.

KEY WORDS: Phase shift, Kainate, Coupled networks, Synchronization, Hippocampus.

Mesial temporal lobe epilepsy (MTLE), the most common form of focal epilepsies in adults, is characterized by seizures originating in temporal lobe structures. It is typically attributed to the hippocampal network and often associated with hippocampal sclerosis, that is, cell loss in the hippocampus proper and the hilus of the dentate gyrus (DG), granule cell dispersion, and mossy fiber sprouting (Margerison & Corsellis, 1966; Sutula et al., 1989; Houser, 1990). Surprisingly, the sclerotic region alone is not sufficient to generate epileptiform activity (EA, comprising ictal activity during seizures and interictal activity between seizures) in animal models of MTLE in vitro (Le Duigou et al., 2008). Moreover, in a number of patients with MTLE, seizures persist after hippocampal resection (Ryvlin & Kahane, 2005), suggesting that structures other than the hippocampus (HC) are also involved in seizure generation. Several studies have emphasized the involvement of the entorhinal cortex (EC). Indeed, hippocampal sclerosis is often associated with cell loss in the superficial layers of the EC in humans (Du et al., 1993; Yilmazer-Hanke et al., 2000; Bartolomei et al., 2005) and animal models (Du et al., 1995).

Although these structures and their implications for EA generation have been widely studied, their functional connectivity in the epileptogenic network in vivo is still an open issue. EA is a dynamic state clearly different from ongoing activity; however, such changes in interaction should leave a persistent imprint in ongoing activity between EA events. In fact, to understand how EA is initiated, we should know the dynamics of interactions within epileptogenic networks during EA-free ongoing activity. Apart from seizure prediction studies, EA-free activity, typically considered as ''normal'' activity separating EA episodes, has thus far received little attention. The anatomic changes observed in the brain structures involved, however, predict aberrant network activity not only during EA, but also during EA-free periods.

To identify signatures of these changes on the network level, we focused on the interaction between EC and DG as the input stage of the hippocampal network during EA-free periods. We simultaneously recorded local field potentials

Accepted July 27, 2012; Early View publication September 17, 2012.
Address correspondence to Ulrich Egert, Biomicrotechnology, Department of Microsystems Engineering, IMTEK, Faculty of Engineering, Albert-Ludwigs University Freiburg, Georges-Koehler-Allee 102, 79110 Freiburg, Germany. E-mail: egert@imtek.uni-freiburg.de

Wiley Periodicals, Inc.

(LFPs) in the DG and the EC in the intrahippocampal kainate (KA) mouse model of MTLE (Bouilleret et al., 1999; Heinrich et al., 2006; Meier et al., 2007). We show that KA injection introduces delayed synchrony between LFPs in the medial EC (MEC) and the DG during EA-free ongoing activity, most prominent in the theta band. To identify possible underlying mechanisms, we implemented a computational neural mass model that incorporates the KA-induced anatomic changes. The model suggests that pathologic changes in the HC suffice to introduce a temporal shift within the EC–HC loop, consistent with the experimental data.

Materials and Methods

Animals

All animal procedures were in accordance with the German Animal Welfare Act and were approved by the ethics committee of the regional council in Freiburg, Germany. Mice were kept at 22 ± 1°C in a 12 h light/dark cycle with food and water ad libitum.

Injections

Eighteen adult male C57Bl/6 mice (7–10 weeks; Biomed Center, University of Freiburg, Freiburg, Germany) were anesthetized (ketamine hydrochloride 100, xylazine 5, atropine 0.1 mg/kg body weight, i.p.) and mounted into a stereotaxic frame (David Kopf Instruments, Tujunga, CA, U.S.A.). In 14 mice, KA solution (50 nl, 20 μM in 0.9% NaCl; Tocris, Bristol, U.K.) was injected locally into the right dorsal DG as described previously (Heinrich et al., 2006, coordinates from bregma (mm): rostro-caudal (RC) = −2.0, medio-lateral (ML) = −1.5, dorso-ventral (DV) = −1.9). Similarly, four control mice were injected with the same amount of 0.9% sterile NaCl.

Electrophysiology

Two weeks after injection, when recurrent EA can be reliably recorded and hippocampal sclerosis is prominent (Bouilleret et al., 1999; Heinrich et al., 2006; Häussler et al., 2012), five KA and four NaCl mice were reanesthetized, and steel electrodes with polyester isolation (ø 125 μm, FE245840; Goodfellow Cambridge Ltd., Huntingdon, U.K.) were implanted into DG and MEC (coordinates from bregma (mm): DG: RC = −2.0, ML = −1.5, DV = −1.9; EC: RC = −4.6 ML = −2.8, DV = −3.6), fixated and soldered to a connector for chronic LFP recordings. In two KA mice, an additional electrode was implanted into CA1 (coordinates from bregma [mm]: RC = −3.3, ML = −2.9, DV = −2.7) and one further KA mouse had electrodes in DG and CA1 only. Reference electrodes were implanted subcranially above the cerebellum. Implantation of the reference above the prefrontal cortex showed comparable results, which confirmed independence of reference position.

LFP recordings were performed every second day for up to 3 weeks (1,000× amplification, 1–5,000 Hz bandpass [MPA8I + PGA32; Multichannel Systems, Reutlingen, Germany], sampling frequency 10 kHz [Power 1401 mk2, spike2 software, CED, Cambridge, U.K.]). Animal behavior was monitored with a video camera. Following the last recording session, mice were anesthetized and transcardially perfused with 4% paraformaldehyde. To verify electrode positions and granule cell dispersion (if applicable), brains were sectioned (sagittal plane, 70 μm) and stained with cresyl violet as previously described (Heinrich et al., 2006).

Tests for cell loss

To test for neuronal degeneration in HC and MEC, six KA mice without electrodes were sacrificed at different time points after KA injection (7 and 21 days [n = 2 each], 2 and 14 days [n = 1 each]). Sections (sagittal plane, 70 μm) were mounted on gelatin-coated slides, air-dried, transferred into 0.06% potassium permanganate solution, washed in distilled H_2O, and stained with 0.0004% Fluoro-Jade B (FJB; Chemicon, Temecula, CA, U.S.A.) solution. Sections were cleared in xylene and mounted with Hypermount (ThermoShandon, Dreieich, Germany). All sections were photographed with appropriate filter sets and equal exposure times. To quantify cell loss, images taken from sections at 7 and 21 days after KA injection (one image per position for each mouse and time point) were analyzed using ImageJ (Wayne Rasband, NIH, Bethesda, MD, U.S.A.). HC and MEC where marked in the images, followed by calculation of the mean and standard deviation (SD) of gray values in the HC. We defined pixels as FJB-positive if their gray values exceeded mean + 3*SD. This threshold was applied to both HC and MEC, and the number of pixels with intensity above threshold was measured and set relative to the total area.

To further test for cellular changes in the MEC, the brains of two naive and two KA mice (21 days after KA) were sectioned (horizontal plane, 50 μm) and subjected to Nissl staining and immunocytochemistry for Reelin, as described previously (Gross et al., 2012). In brief, we used a mouse-on-mouse kit (M.O.M. Basic Kit BMK-2202; Vector Laboratories, Burlingame, CA, U.S.A.) following the manufacturer's instructions, anti-Reelin antibody (G-10, 1:1,000; Millipore, Bedford, MA, U.S.A.), and development with 3,3′-diaminobenzidine (DAB; Sigma-Aldrich, Taufkirchen, Germany).

Data analysis

We performed all data analyses in Matlab 2011a (TheMathworks, Natick, MA, U.S.A.). To calculate spectrograms, we estimated the short-time Fourier transform of the raw samples (Hamming window, 60 msec segment size, 25% overlap between segments).

For correlation analysis, data were resampled to 2 kHz and filtered in the respective target bands (theta: 4–8, alpha: 8–12, beta: 12–30, low gamma: 30–45 Hz, second order

Butterworth filter). The last 15 min of each recording from control mice were cut into 50-s epochs. In recordings from KA mice, EA-free epochs were cut with a dead-time of 1 s before and after EA by applying a threshold on the DG signals. KA data segments were used for further analysis if their duration was ≥ 23 s.

To check the relation of MEC and DG signals, time-resolved cross-correlograms (TRCCs) were computed for the filtered MEC (x) and DG (y) signals in a sliding window (2 s duration, shifted by 250 msec). The stationarity of the delayed synchrony was confirmed by pair-wise linear correlation of the mean cross-correlogram of the first recording and subsequent recordings. Mean cross-correlograms of each mouse in the theta band were calculated after pooling all 2-s cutouts. Distributions of the maximal correlation values (ρ_{max}) and the lag values (Δt_{peak}) were computed by detection of ρ_{max} within a time frame of −90 to +90 msec in theta band and generation of the cumulative histograms. These were normalized by point-wise division with their cumulative sum. To compare the different frequency bands, Δt_{peak} values were converted into corresponding phases. Phase at zero lag was calculated with respect to the first positive peak in the cross-correlogram, which was assigned to zero phase. The phase and correlation of the cross-correlograms are represented in polar coordinates as a two-dimensional probability density function.

Computational model

Computer simulations were performed using a lumped-parameter model of coupled neuronal populations, proposed by Jansen and Rit (1995). A full description of the model is provided in the supplementary data. In brief, the model comprises two neuronal populations, which were considered here as surrogates for the EC (population 1) and the HC (population 2). Their parameters (related to neuronal excitability and connectivity) were set so that they both produced theta band activity (see Fig. S4). They were mutually connected by excitatory synaptic connections between the principal cell subpopulations (Jansen & Rit, 1995). Interactions between the two populations were characterized by two coupling coefficients, $K_{EC\rightarrow HC}$ and $K_{HC\rightarrow EC}$, which represent the strength of the connection from one population to the other. We modeled cell loss by varying the coefficients between the two populations between 0 and 500 (increments of 25). Due to the symmetry of the system, exploration of the two-dimensional parameter space was restricted to values such that $K_{HC\rightarrow EC} \leq K_{EC\rightarrow HC}$. For each couple ($K_{EC\rightarrow HC}$, $K_{HC\rightarrow EC}$), we simulated LFPs produced by the populations, calculated TRCCs, and estimated ρ_{max} and Δt_{peak}.

Results

All KA mice showed a clear status epilepticus after injection, as described previously (Riban et al., 2002), and the success of the injection was confirmed by verification of the dispersion of the granule cell layer (GCL) in the septal HC in Nissl-stained sections (Fig. 1C). Control mice showed neither a status epilepticus nor a granule cell dispersion.

Epileptiform activity in the MEC

To investigate the functional connectivity between MEC and DG during EA-free periods, we implanted electrodes for LFP recordings targeting layer II of the MEC (Fig. 1C, left) and into the GCL of the DG in five KA-injected and four NaCl-injected mice (Fig. 1C, right).

All recordings in KA mice (n = 36) clearly showed EA at the DG as described previously (Bouilleret et al., 1999). It was characterized by major asymmetric excursions from baseline activity, similar to dentate spikes (Bragin et al., 1995) but repeatedly followed by the same pattern (Fig. 1A, top). Simultaneously with the DG, we observed EA in the MEC as well, indicating involvement of both structures in EA generation.

In each recording session, EA appeared with high rate (∼2 events per minute, with durations of 2 s or longer). These events were not associated with discernible changes in animal behavior but visible in the LFP recordings only, apart from rare generalized behavioral seizures. In the following analyzes, any interictal, ictal, and postictal activity was excluded as we focused on the activity between EA in KA mice and ongoing activity in controls.

No apparent differences in ongoing activity within DG and MEC

We extracted 772 EA-free epochs from 36 recordings from five KA mice (median duration 31.5 s, range 23–337 s). Similarly, 378 epochs of comparable duration (50 s each) were extracted from 21 recordings from four control mice. Visual inspection of these epochs revealed no apparent differences in spectral and temporal composition in the MEC and DG ongoing activity between control and KA mice (Fig. 1A,B), apart from an overall reduced amplitude and power in the DG of the latter that we attribute to cell loss and granule cell dispersion. Hence, we analyzed the ongoing activity in both groups in more detail.

Delayed synchrony between MEC and DG in KA mice

We first restricted analysis to the theta band (4–8 Hz), because theta band oscillation in the LFP is a prominent feature in the hippocampal formation in several behavioral states (Buzsáki et al., 1986; Alonso & García-Austt, 1987). Moreover, the theta rhythm is considered to be involved in memory functions (Hasselmo et al., 2002), which are impaired under epileptic conditions (Hoppe et al., 2007; Gröticke et al., 2008).

We calculated TRCCs between the LFPs recorded in the MEC and the DG for theta band filtered signals. In all mice, TRCCs showed a pronounced anticorrelation of activity in MEC and DG (Fig. 2A,B, cf. Fig. S1 for raw and filtered traces). On average, in control mice, the maximal

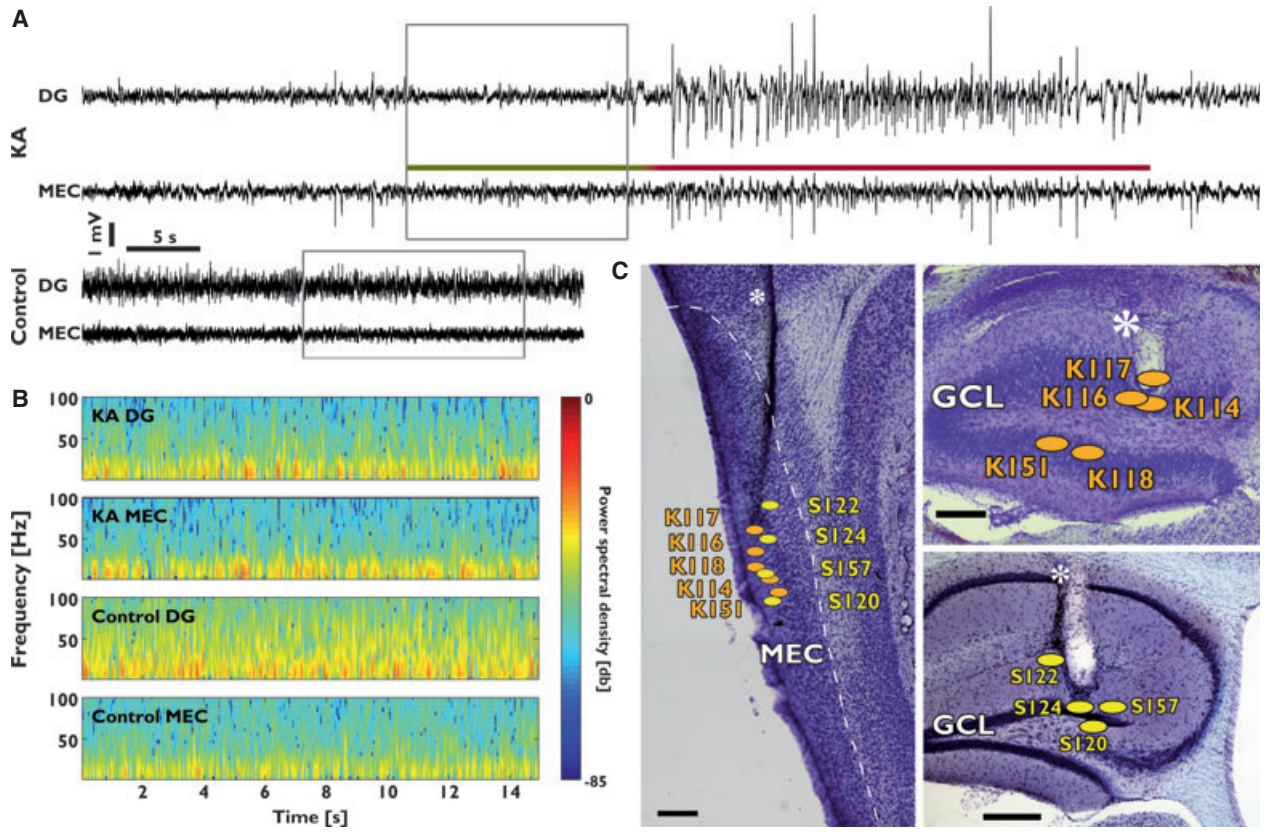

Figure 1.

EA-free activity from KA-injected mice is comparable to control activity. (**A**) Example traces from KA (K117, top) and control (S124, bottom) mice, simultaneously recorded at the injection site (DG) and the MEC. In KA traces, the green horizontal line indicates a period without EA, followed by a transition into an EA event (red) at both recording sites. Control traces show normal ongoing activity. (**B**) Spectrograms calculated for 15-s cutouts from above traces (gray boxes in A). The spectral composition of activity up to 100 Hz of KA mice is comparable to control activity. (**C**) Electrode positions for all mice. Electrode tracks are indicated by white stars, scalebars = 200 μm. Left: Positions of entorhinal electrodes, superimposed on a representative Nissl-stained section (mouse K117). The border of the EC is indicated by the white dashed line. Right: Positions of electrodes at injection site in KA (top, mouse K114) and control (bottom, mouse K124) mice. Note the dispersed granule cell layer (GCL) in the KA section when compared to the control section.

correlation values (ρ_{max}) occurred near zero time lag ($\Delta t_{peak} \approx 0$ msec, Fig. 2A). In contrast, in KA mice, LFPs in the MEC and DG were correlated with a positive lag, indicating that MEC activity lagged behind the DG during EA-free ongoing activity (Fig. 2B). These Δt_{peak} values persisted throughout a recording session (mean duration 108 min, epochs 23–100 s; Fig. 2C), independent of changes in ρ_{max}. In both animal groups the parameters ρ_{max} and Δt_{peak} were highly stable (Fig. S2). To assess the long-term stability of the delayed synchrony, we calculated the mean cross-correlogram for all recordings and the pairwise linear correlation between the first and subsequent recordings, which were highly correlated over weeks (Figs. 2D and S3, correlation coefficient ≥ 0.7). We therefore pooled all epochs from all recordings from each mouse and calculated the respective mean cross-correlograms (Fig. 3A). This clearly demonstrated that delayed synchrony between MEC and DG during ongoing activity is specific to KA mice (overall $\Delta t_{peak} = 24.4 \pm 27.7$ ms (mean ± SD). We did not observe comparable delays in control animals (overall $\Delta t_{peak} = 0.1 \pm 24.9$ ms). Distributions of Δt_{peak} (Fig. 3B, left) for each animal further confirmed that ongoing activity in KA mice was marked by delayed synchrony, with no appreciable difference in ρ_{max} (Fig. 3B, right).

To identify whether the delayed synchrony between MEC and DG was restricted to the theta band, we calculated the ρ_{max} and Δt_{peak} for four behaviorally relevant frequency bands, represented as two-dimensional histograms in polar coordinates (Fig. 3C). In these, the angle translates to the phase (φ) of the cross-correlogram at 0 msec time lag and the radius refers to the corresponding ρ_{max}. In the theta band, the dominant frequency in the cross-correlograms had a period of ≈170 msec, a delay of $\Delta t_{peak} \approx 24$ msec in the KA mice thus results in a shift of ≈50 degrees. We further

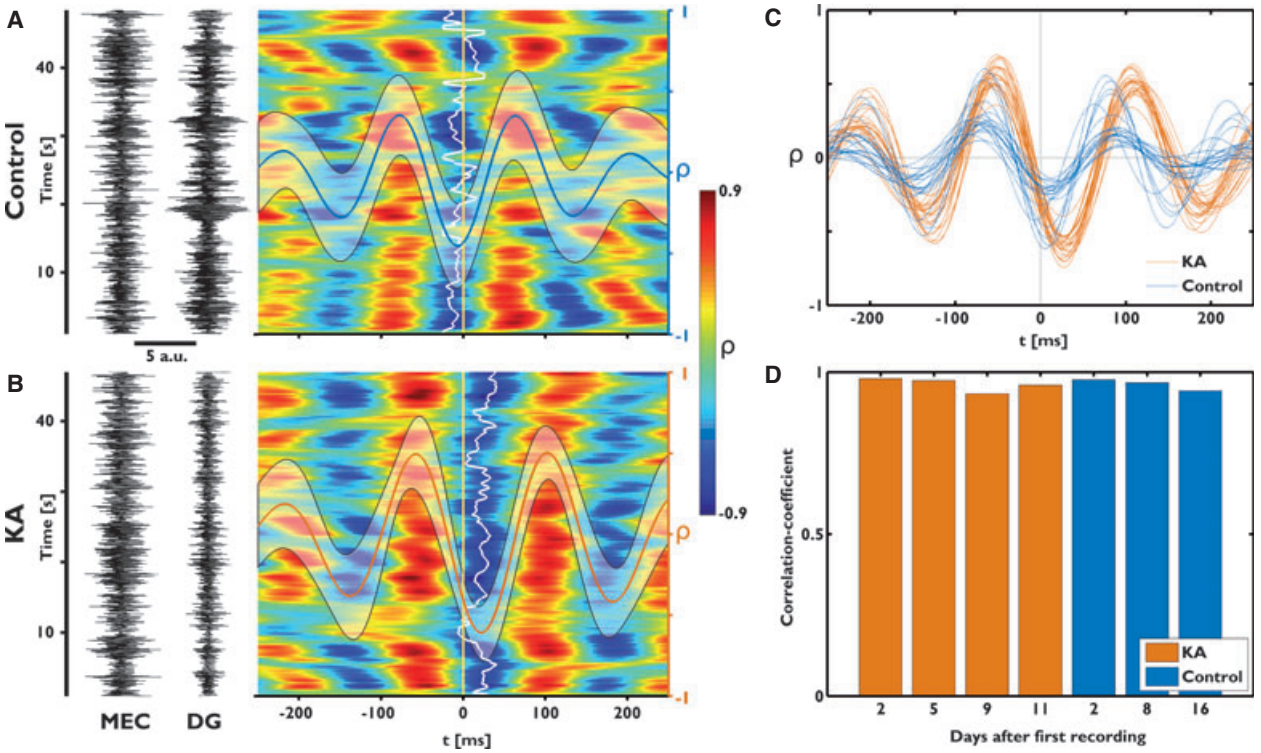

Figure 2.

Correlation analysis in theta band of KA data shows a positive lag between MEC and DG when compared to control data. (**A**) Left: Example epoch with ongoing activity from MEC and DG electrodes in a healthy control mouse (S120) after filtering in theta band (4–8 Hz). Right: Time-resolved cross-correlation (TRCC) result (ρ: correlation-coefficient, t: lag) from this epoch (pseudo-color map, time axis is the same as for the traces) with the mean (blue line, right *y*-axis) and standard deviation (transparent surface) of ρ superimposed (right *y*-axis gives coefficient). Each horizontal line in the pseudo-color plot is the result from cross-correlating 2 s of the filtered MEC signal with the filtered DG signal. The evolution over time results from sliding these 2-s cutouts by 250 msec until maximum time of the epoch is reached. The vertical white line follows the maximal anti-correlation to estimate the jitter, the yellow line indicates t = 0 and thereby 0 msec lag. The mean of the correlation result displays its highest absolute ρ-value close to 0 msec lag (i.e., $\Delta t_{peak} \approx 0$ ms). (**B**) Same as A, but with EA-free signals from a KA-injected mouse (K116) and the line representing the mean in red. The highest mean correlation is at $\Delta t_{peak} \approx 23$ msec. (**C**) Mean of the correlation results from all epochs from one recording session for K116 (orange, $\Delta t_{peak} \approx 24$ msec) and S120 (blue, $\Delta t_{peak} \approx 0$ msec). The Δt_{peak} values of KA and control persist over epochs. (**D**) Stability of the average cross-correlation results from all epochs from given recordings over weeks. The bars give the pairwise linear correlation of the mean correlation result of the first recording with following recordings as a measure of similarity in the two mice (for group data see Fig. S3).

found a phase difference in the alpha band (8–12 Hz) but with lower ρ_{max}. In higher frequency bands, activity in MEC and DG was uncorrelated (Fig. 3C). Thus, EA-free ongoing activity in the MEC and DG is temporally mismatched as compared to healthy mice in low frequency bands. Because of this restriction, we analyzed the behavior of the mice in phases where the shift was most distinct. During these phases, KA mice showed exploratory behavior. Comparably, control mice were exploring when synchronized theta band activity was most pronounced.

Neuronal degeneration in HC, but not in MEC

What could cause the shift of MEC and DG signals in epileptic mice? We hypothesized that it results from changes in the coupling of MEC and DG, mediated by neuronal loss in the EC-HC loop. Intense FJB labeling at several time points after KA injection (2, 7, 14, 21 days) revealed strong neuronal degeneration in the HC, which we confirmed by densitometric quantification of fluorescence intensity (7, 21 days after KA; Fig. 4A,C). Although the MEC was involved in EA, we did not detect any neuronal degeneration in the MEC in KA-injected mice at any time point (Fig. 4B,C).

Because FJB stains only acutely degenerating neurons, we could not exclude that cells were already lost within the first few hours after KA injection. To test for this, we additionally performed Nissl stainings and Reelin immunocytochemistry at 21 days after KA injection. Reelin expression has been found in the EC exclusively in layer II in cells

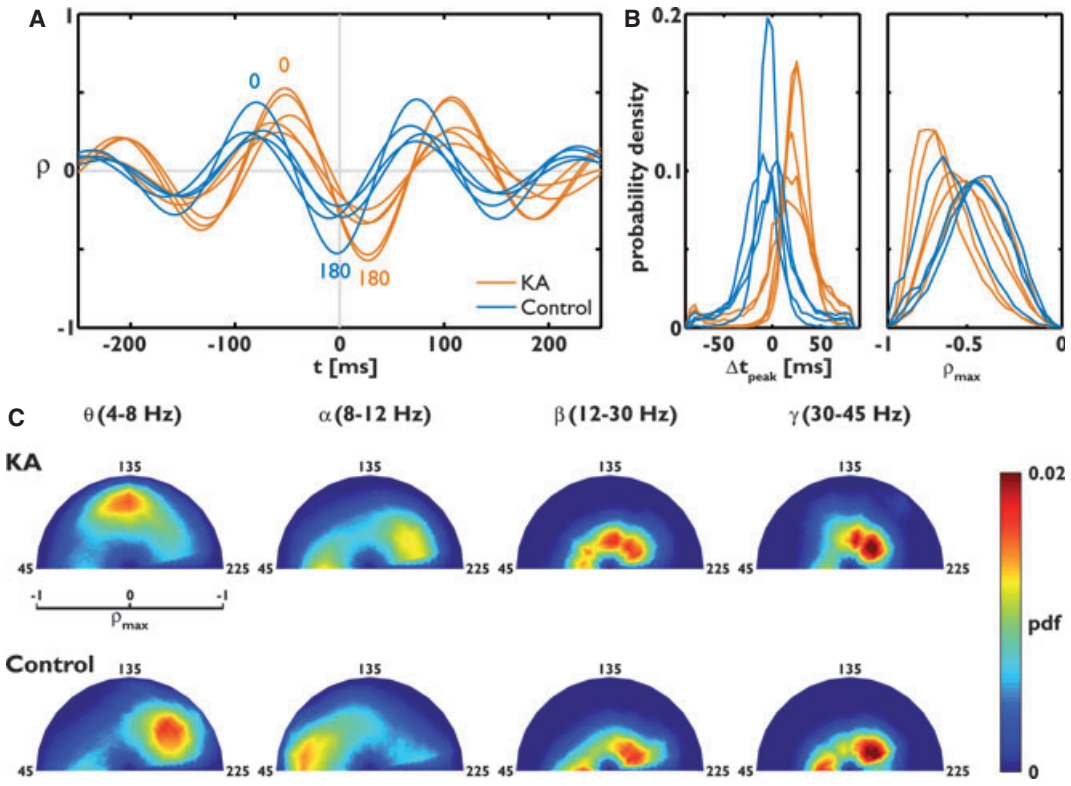

Figure 3.

A phase lag appears in all KA mice, but vanishes in frequency bands higher than theta band. (**A**) As the findings persisted over weeks, we calculated the mean of all correlation values of all recordings from each mouse (KA: orange, control: blue). All KA-injected mice showed a positive lag ($\Delta t_{peak} \approx 24$ msec) for the DG, whereas in all control mice Δt_{peak} appeared around 0 msec lag. The 0 degree and 180 degrees are referred to in panel C. (**B**) Left: Distribution of all Δt_{peak} values from both, KA (orange) and control (blue) mice (evaluation window of −90 to 90 msec). Right: Same as left but for the corresponding ρ_{max} values. (**C**) We detected the first positive peak correlation before 0 msec lag and set it to 0 degrees, as well as the first negative peak after 0 msec to 180 degrees (cf. panel A). In this way, we estimated the phase (φ) at 0 msec lag of all 2-s cutouts without averaging. The polar plots represent φ with its corresponding ρ_{max} as radius resulting in a polar two-dimensional probability density function (pdf). The KA Δt_{peak} around 24 msec in the theta band translated into a ∼50-degree phase shift when compared to controls. Evaluating higher frequency bands resulted in a decreased correlation and a progressively vanishing shift.

projecting to the DG via the perforant path (Varga et al., 2010). Our stainings revealed comparable density of Reelin-expressing cells in layer II in KA-injected and naive mice and no obvious changes in the cortical layers, (Fig. 4D).

Therefore, we assumed that the connections from MEC to DG were preserved, except for changes of the local network in the DG. Consequently, hippocampal cell loss could result in a reduced coupling from the HC to the MEC.

Imbalanced coupling between two neuronal populations leads to delayed synchrony

To test whether reduced coupling between HC and EC can suffice to induce delayed synchrony, we performed computer simulations using a model of two coupled neuronal populations (based on Jansen & Rit, 1995; Fig. 5A). We considered the EC as one population and lumped all hippocampal subfields including DG and subiculum into a second population (HC). We systematically varied $K_{EC\to HC}$ and $K_{HC\to EC}$ coefficients to investigate the effect of the interpopulation coupling strength on the synchrony between EC and HC populations. Figure 5B,C show ρ_{max} and Δt_{peak} for the simulated HC and EC LFPs in the theta band as a function of interpopulation connectivity. When the two populations were coupled with comparable connection strengths (i.e., $K_{EC\to HC} \approx K_{HC\to EC}$; along the diagonal in Fig. 5B), EC and HC activities were synchronized with near zero time lag (−0.2 ± 2.9 msec [mean ± SD], Fig. 5C). When the feedforward connection to the HC was stronger than the feedback connection to EC (i.e., $K_{EC\to HC} > K_{HC\to EC}$; e.g., $K_{EC\to HC} = 120$ and $K_{HC\to EC} = 10$, Fig. 5B), EC activity was phase delayed by ≈16 msec (15.6 ± 8.8 msec, Fig. 5C). Therefore, the model

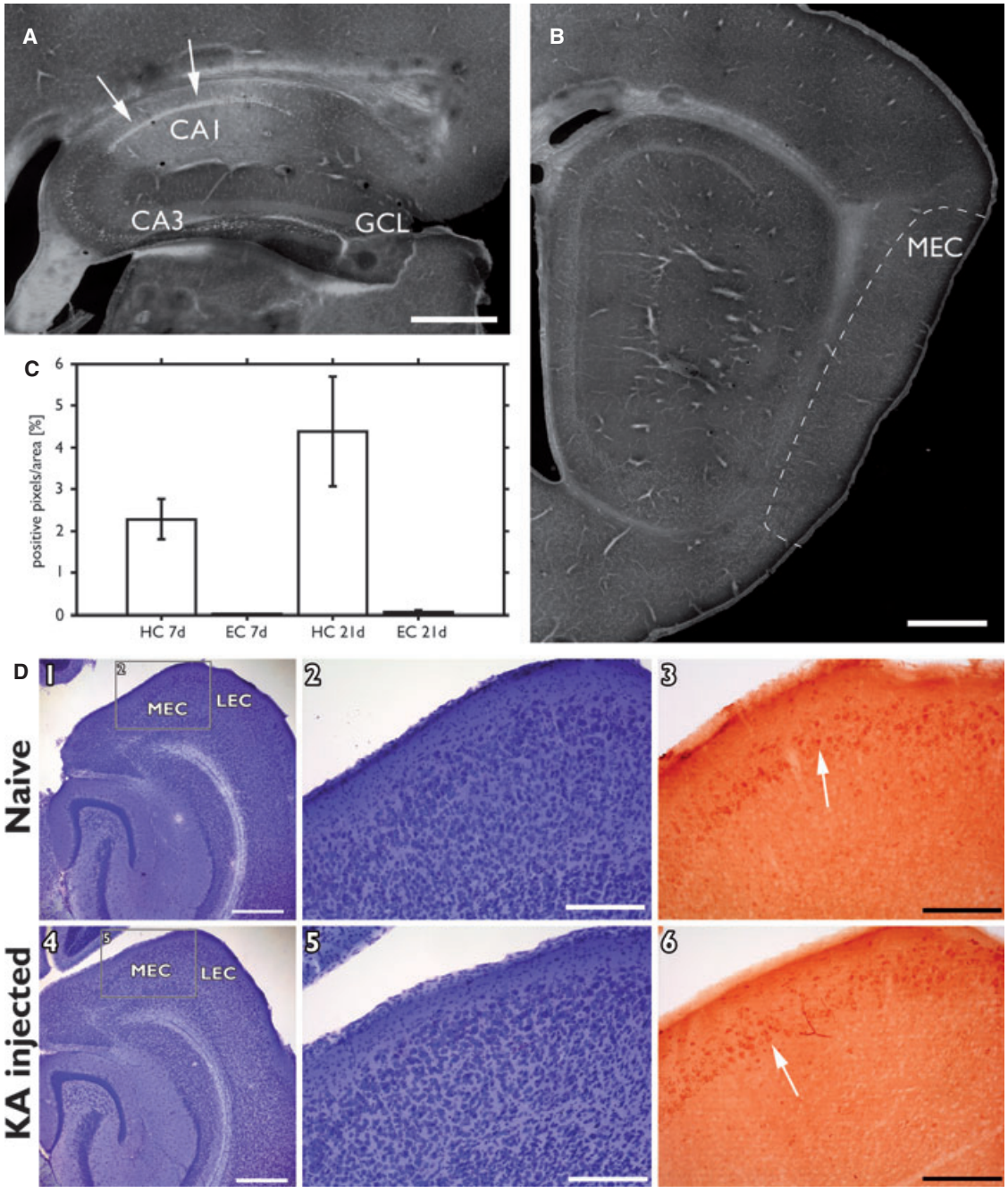

Figure 4.

No apparent neuronal degeneration in the MEC. (**A**) After focal injection of KA (here: 7 days), neuronal degeneration was observed in areas CA3 and CA1 (sagittal sections, FJB staining, arrows indicate examples). (**B**) In contrast, the MEC lacks FJB-stained cells between 2 and 21 days after KA (here: 7 days, same mouse as in A). The dashed line indicates the border of the MEC. (**C**) By applying a threshold on the FJB-positive pixels in the HC, these were counted and normalized to the area to quantify the amount of degeneration 7 and 21 days after injection (n = 2 per time point, mean ± SD). (**D1**) Cutout of a Nissl-stained horizontal slice of a naive mouse including the MEC and the lateral EC (LEC). The frame indicates the borders of the magnification (**D2**), which shows layering of the MEC. (**D3**) A cutout comparable to (D2) of a immunocytochemical staining for Reelin from the same naive mouse shows Reelin-positive cells in the superficial MEC (arrow indicates example). (**D4**) Same as (D1) but from a KA-injected mouse, 21 days after injection. (**D5**) There were no distinct differences in cell density in the MEC as compared to the naïve mouse. (**D6**) Similarly, immunocytochemistry for Reelin revealed no difference (arrow indicates example; scalebars: (A)-(D1) and (D4) = 500 μm, else 200 μm). Note that in the slicing plane in (D), the intermediate hippocampus does not show distinct anatomic changes.

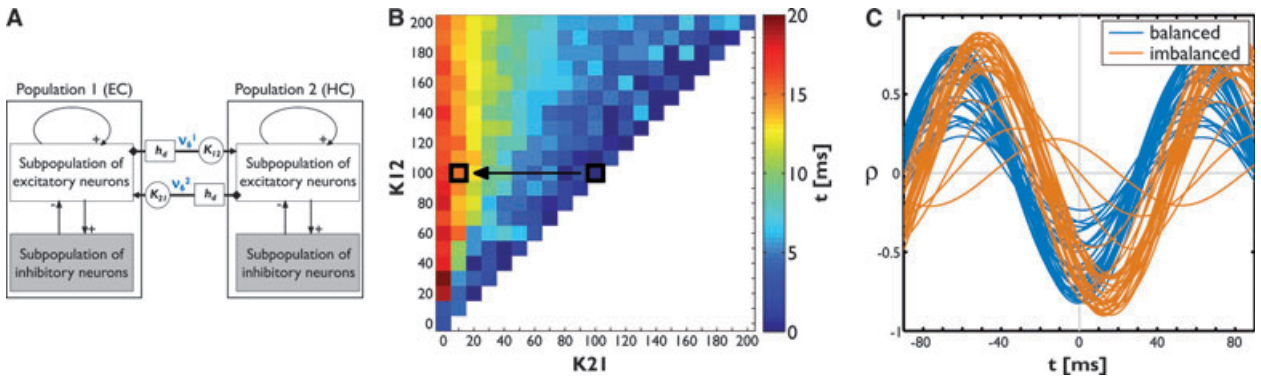

Figure 5.
The computational model supports coupling imbalance as a mechanism for phase shift. (**A**) Schematic representation of the computational model of two coupled neuronal populations. (**B**) A color map of Δt_{peak} (i.e., the lag of the highest negative correlation value) as a function of $K_{EC\rightarrow HC}$ (*y*-axis) and $K_{HC\rightarrow EC}$ (*x*-axis) coupling coefficients. Each colored element was obtained from 30 simulations of pairs of population (LFP-like) signals (25-s duration) and corresponds to the mean of the Δt_{peak} values estimated for these 30 simulations. Note that due to the symmetry of the system, the exploration of the two-dimensional parameter space was restricted to values such that $K_{EC\rightarrow HC} \leq K_{HC\rightarrow EC}$. (**C**) Mean of the correlation from 30 simulations, for a balanced coupling between the two populations (blue, corresponding to $K_{EC\rightarrow HC}$ = 120 and $K_{HC\rightarrow EC}$ = 120) and for an imbalanced coupling (orange, corresponding to $K_{EC\rightarrow HC}$ = 120 and $K_{HC\rightarrow EC}$ = 10). The highest correlation-coefficients occurred at −0.2 ± 2.9 msec lag in the former case and at 15.6 ± 8.8 msec lag in the latter case (mean ± SD).

strongly supports the hypothesis that hippocampal cell loss reduced the connectivity from the HC to the EC and that this introduces the temporal lag between these networks during EA-free activity.

Discussion

We analyzed the phase relation between ongoing oscillatory LFP activity in layer II of the MEC and the dentate GCL in epileptic mice to identify the signature of structural network changes in EA-free ongoing dynamics. In contrast to healthy mice, where the phase relation between MEC and DG theta activity was close to zero, theta- and alpha-band synchronization were delayed in epileptic mice during EA-free episodes. We suggest that this temporal mismatch is caused by an imbalance of the polysynaptic connectivity between the EC and the HC, based on the computational model of the EC-HC network. A likely cause of imbalance is the cell loss throughout the HC, whereas the MEC appeared intact.

Epileptiform activity occurs in HC and MEC

Recent evidence suggests that even in partial epilepsies, different brain regions could act as independent generators of EA and initiate seizure episodes (Bertram, 2009). Consistent with observations in patients with MTLE (Bragin et al., 1999; Bartolomei et al., 2005), our recordings revealed EA in the MEC, even though KA was injected focally into the DG. Because the EC is the main source of cortical input to the HC, EA is relayed to the HC. This suggests that the EC plays a crucial role in shaping EA dynamics.

Although we cannot exclude that the MEC is affected by changes too subtle for the histologic analyzes applied, we did not find obvious signs of neuronal degeneration over 3 weeks after KA injection. This is striking because several studies on animal models showed cell loss in the MEC (Du et al., 1995; Wozny et al., 2005; Kumar & Buckmaster, 2006; Tolner et al., 2007; Zahn et al., 2008). In contrast to our experiments, however, the epileptic condition was induced by systemic application of excitotoxic agents in these studies. This affects extended brain regions and can thus explain the difference. Cell loss in the EC after focal injection of pilocarpine into the DG of rats, as shown in a recent study (Castro et al., 2010), might result from differences between the receptors targeted by the epileptogenic agents as well as species differences (Buckmaster, 2004). Prominent cell loss in the hippocampus in our study is in accordance with previous reports (Heinrich et al., 2006) and leads to permanent changes in the network structure, which likely set the stage for the occurrence of EA (Dalby & Mody, 2001; Tang & Loke, 2009). Functional signatures of these changes, however, could be masked during EA, but be visible in the activity between seizures.

Delayed synchrony in KA mice

The cellular changes in KA mice can affect temporal interactions between subpopulations in the EC-HC loop. The MEC and the DG theta band LFPs from healthy mice were correlated with near zero time lag, which is consistent with recordings in rats (Alonso & García-Austt, 1987; Dickson et al., 1994). The delayed synchrony of ≈24 msec

between MEC and DG in epileptic mice appeared to be specific for the theta band, although a delay could also be observed in the alpha band but with decreased ρ_{max}.

In both groups, TRCC analyzes showed the ρ_{max} values at negative correlation, that is, the signals were anti-correlated (cf. Fig. 2A,B). Such an inversion has also been found between DG and MEC in the rat (Chrobak & Buzsáki, 1998) and might depend on electrode position with respect to somatic or dendritic regions. The DG electrodes in the current work were positioned very close to the somatic regions in the GCL. For the DG, no inversion of signals between layers has been reported (Buzsáki et al., 2003). For MEC layer II, however, a ''reversal zone'' has been shown where signals close to layer I are inverse to signals close to layer III (Chrobak & Buzsáki, 1998). Furthermore, activity during EA in KA mice was antiphasic as well (see Fig. 1A). In addition, in mice with CA1 electrodes, we reconstructed the positions in the dendritic field and signals showed an inverse polarity between CA1 and DG (Fig. S3). These findings confirm that the inversion between MEC and DG signals and the corresponding negative ρ_{max} result from electrode positions.

The observation of delayed synchrony only at frequencies between 4 and 12 Hz may be attributed to the findings that activity in higher frequency bands synchronizes only temporarily and with high variability between hippocampal structures (Chrobak & Buzsáki, 1998; Colgin et al., 2009). Finally, preliminary analysis revealed delayed theta synchrony also during EA (data not shown), however, this is confounded by drastic changes of spectral and temporal LFP features, and these phases are not comparable to ongoing activity in healthy mice.

Origin of delayed synchrony

Because the MEC provides the main cortical input to the DG, it is counterintuitive that activity in the MEC is delayed with respect to the DG. In a feed-forward system, one would expect that activity in the presynaptic network leads the activity in the postsynaptic network. The EC and HC, however, form a recurrent network where hippocampal output is sent back to the deep layers of the EC. In such a system, it is not straightforward to assign a particular network to be presynaptic, especially when based on band-limited LFP signals.

It is known that in synchronized coupled linear systems, a phase shift can arise due to mismatch in the connectivity between the participating systems (Strogatz, 2000). We hypothesized that this also holds for the EC-HC loop and that the temporal mismatch may arise from imbalanced coupling between these structures, for example, through structural changes in one of the subnetworks.

We tested this in a computational model of two coupled neuronal populations representing the HC and the EC. Their activity was simulated using a ''neural mass'' modeling approach (Wilson & Cowan, 1972; Lopes da Silva et al., 1974; Freeman, 1978), which describes the average activity of neural ensembles without explicitly representing individual neurons. We chose such a mesoscopic model because it generates activity analogous to LFPs and hence can be compared directly to our recordings. The lumping of all subfields of HC into one population was motivated by the observation of zero lag correlation between CA1 and DG (Fig. S3 for KA mice), suggesting that the DG (as hippocampal input) and CA1 (as output region) are synchronized. Moreover, in a closed-loop network consisting of two or more neural populations, changes in connectivity between any two populations would result in qualitatively similar results.

As a consequence of cell loss in the HC, although we did not find cell loss in the MEC, the number of connections from MEC to HC in epileptic mice might be similar to controls, whereas the septal HC to MEC projections might be significantly reduced, resulting in imbalanced connectivity between the two structures. Consistent with this, the simulations showed that balanced coupling between the two populations yields zero time lag synchrony, whereas imbalanced coupling (obtained by decreasing the strength of the connection from one population to the other) yielded a positive time lag. This model therefore presents a mechanism by which cell loss in the HC can lead to delayed synchrony. Whether the connection from MEC to HC, however, is in fact comparable in both animal groups should be tested in the future.

Based on the structure of our computational model, we suggest that the temporal mismatch between EC and HC activity does not require a loss of connectivity at a particular subfield. Altered connectivity at any location in a looped network could change the temporal relationship between subfields. This is consistent with the observed heterogeneity of the focus of EA and location of sclerosis in patients with MTLE and animal models (Bertram, 2009). In addition, this view is supported by epileptic seizures occurring after chemically induced restricted lesions in the EC with cell loss limited to the EC (Brun et al., 2008).

Implications for epilepsy

The observation of delayed synchrony particularly in the theta band is remarkable because the theta band activity in the hippocampal formation is strongly related to the spiking activity and thought to underlie memory formation (O'Keefe & Recce, 1993; Huxter et al., 2003; Nadel & Hardt, 2004; Buzsáki, 2006; Hafting et al., 2008). Therefore, a temporal mismatch in theta band LFP between the MEC and the DG activity suggests that in KA mice, MEC inputs to the DG differ from controls, which might explain memory deficits (Gröticke et al., 2008), impaired place cell activity, and phase precession (Lenck-Santini & Holmes, 2008) under epileptic conditions.

Moreover, if spiking activity associated with the theta band LFP in the MEC of KA mice would also be delayed with respect to spiking activity in the DG, synaptic strengthening could render the whole EC-HC loop prone to EA generation.

To test this hypothesis, however, we will need to identify the temporal relationship of the spiking activities in the two brain regions.

Acknowledgments

This work was supported by the German Federal Ministry of Education and Research (BMBF, FKZ 01GQ0420 and 01GQ0830) and by the Deutsche Forschungsgemeinschaft (DFG, SFB TR3 and SFB 780). We thank Ad Aertsen, Michael Frotscher, and Imre Vida for their helpful comments.

Disclosure

None of the authors has any conflict of interest to disclose. We confirm that we have read the Journal's position on issues involved in ethical publication and affirm that this report is consistent with those guidelines.

References

Alonso A, García-Austt E. (1987) Neuronal sources of theta rhythm in the entorhinal cortex of the rat. I. Laminar distribution of theta field potentials. *Exp Brain Res* 67:493–501.

Bartolomei F, Khalil M, Wendling F, Sontheimer A, Régis J, Ranjeva JP, Guye M, Chauvel P. (2005) Entorhinal cortex involvement in human mesial temporal lobe epilepsy: an electrophysiologic and volumetric study. *Epilepsia* 46:677–687.

Bertram EH. (2009) Temporal lobe epilepsy: where do the seizures really begin? *Epilepsy Behav* 14(Suppl. 1):32–37.

Bouilleret V, Ridoux V, Depaulis A, Marescaux C, Nehlig A, Le Gal La Salle G. (1999) Recurrent seizures and hippocampal sclerosis following intrahippocampal kainate injection in adult mice: electroencephalography, histopathology and synaptic reorganization similar to mesial temporal lobe epilepsy. *Neuroscience* 89:717–729.

Bragin A, Jandó G, Nádasdy Z, van Landeghem M, Buzsáki G. (1995) Dentate EEG spikes and associated interneuronal population bursts in the hippocampal hilar region of the rat. *J Neurophysiol* 73:1691–1705.

Bragin A, Engel J, Wilson CL, Vizentin E, Mathern GW. (1999) Electrophysiologic analysis of a chronic seizure model after unilateral hippocampal KA injection. *Epilepsia* 40:1210–1221.

Brun VH, Leutgeb S, Wu HQ, Schwarcz R, Witter MP, Moser EI, Moser MB. (2008) Impaired spatial representation in CA1 after lesion of direct input from entorhinal cortex. *Neuron* 57:290–302.

Buckmaster PS. (2004) Laboratory animal models of temporal lobe epilepsy. *Comp Med* 54:473–485.

Buzsáki G. (2006) *Rhythms of the brain*. Oxford University Press, Oxford.

Buzsáki G, Czopf J, Kondákor I, Kellényi L. (1986) Laminar distribution of hippocampal rhythmic slow activity (RSA) in the behaving rat: current-source density analysis, effects of urethane and atropine. *Brain Res* 365:125–137.

Buzsáki G, Buhl DL, Harris KD, Csicsvari J, Czéh B, Morozov A. (2003) Hippocampal network patterns of activity in the mouse. *Neuroscience* 116:201–211.

Castro OW, Furtado MA, Tilelli CQ, Fernandes A, Pajolla GP, Garcia-Cairasco N. (2010) Comparative neuroanatomical and temporal characterization of FluoroJade-positive neurodegeneration after status epilepticus induced by systemic and intrahippocampal pilocarpine in Wistar rats. *Brain Res* 1374:43–55.

Chrobak JJ, Buzsáki G. (1998) Gamma oscillations in the entorhinal cortex of the freely behaving rat. *J Neurosci* 18:388–398.

Colgin LL, Denninger T, Fyhn M, Hafting T, Bonnevie T, Jensen O, Moser M, Moser E. (2009) Frequency of gamma oscillations routes flow of information in the hippocampus. *Nature* 462:353–357.

Dalby NO, Mody I. (2001) The process of epileptogenesis: a pathophysiological approach. *Curr Opin Neurol* 14:187–192.

Dickson CT, Trepel C, Bland BH. (1994) Extrinsic modulation of theta field activity in the entorhinal cortex of the anesthetized rat. *Hippocampus* 4:37–51.

Du F, Whetsell WO, Abou-Khalil B, Blumenkopf B, Lothman EW, Schwarcz R. (1993) Preferential neuronal loss in layer III of the entorhinal cortex in patients with temporal lobe epilepsy. *Epilepsy Res* 16:223–233.

Du F, Eid T, Lothman EW, Köhler C, Schwarcz R. (1995) Preferential neuronal loss in layer III of the medial entorhinal cortex in rat models of temporal lobe epilepsy. *J Neurosci* 15:6301–6313.

Freeman WJ. (1978) Models of the dynamics of neural populations. *Electroencephalogr Clin Neurophysiol Suppl* 1978:9–18.

Gross CM, Flubacher A, Tinnes S, Heyer A, Scheller M, Herpfer I, Berger M, Frotscher M, Lieb K, Haas CA. (2012) Early life stress stimulates hippocampal reelin gene expression in a sex-specific manner: evidence for corticosterone-mediated action. *Hippocampus* 22:409–420.

Gröticke I, Hoffmann K, Löscher W. (2008) Behavioral alterations in a mouse model of temporal lobe epilepsy induced by intrahippocampal injection of kainate. *Exp Neurol* 213:71–83.

Hafting T, Fyhn M, Bonnevie T, Moser MB, Moser EI. (2008) Hippocampus-independent phase precession in entorhinal grid cells. *Nature* 453:1248–1252.

Hasselmo ME, Bodelón C, Wyble BP. (2002) A proposed function for hippocampal theta rhythm: separate phases of encoding and retrieval enhance reversal of prior learning. *Neural Comput* 14:793–817.

Häussler U, Bielefeld L, Froriep UP, Wolfart J, Haas CA. (2012) Septotemporal position in the hippocampal formation determines epileptic and neurogenic activity in temporal lobe epilepsy. *Cereb Cortex* 22:26–36.

Heinrich C, Nitta N, Flubacher A, Müller M, Fahrner A, Kirsch M, Freiman T, Suzuki F, Depaulis A, Frotscher M, Haas CA. (2006) Reelin deficiency and displacement of mature neurons, but not neurogenesis, underlie the formation of granule cell dispersion in the epileptic hippocampus. *J Neurosci* 26:4701–4713.

Hoppe C, Elger CE, Helmstaedter C. (2007) Long-term memory impairment in patients with focal epilepsy. *Epilepsia* 48(Suppl. 9):26–29.

Houser CR. (1990) Granule cell dispersion in the dentate gyrus of humans with temporal lobe epilepsy. *Brain Res* 535:195–204.

Huxter J, Burgess N, O'Keefe J. (2003) Independent rate and temporal coding in hippocampal pyramidal cells. *Nature* 425:828–832.

Jansen BH, Rit VG. (1995) Electroencephalogram and visual evoked potential generation in a mathematical model of coupled cortical columns. *Biol Cybern* 73:357–366.

Kumar SS, Buckmaster PS. (2006) Hyperexcitability, interneurons, and loss of GABAergic synapses in entorhinal cortex in a model of temporal lobe epilepsy. *J Neurosci* 26:4613–4623.

Le Duigou C, Bouilleret V, Miles R. (2008) Epileptiform activities in slices of hippocampus from mice after intra-hippocampal injection of kainic acid. *J Physiol* London 586:4891–4904.

Lenck-Santini PP, Holmes GL. (2008) Altered phase precession and compression of temporal sequences by place cells in epileptic rats. *J Neurosci* 28:5053–5062.

Lopes da Silva F, Hoeks A, Smits H, Zetterberg LH. (1974) Model of brain rhythmic activity. The alpha-rhythm of the thalamus. *Kybernetik* 15:27–37.

Margerison JH, Corsellis JAN. (1966) Epilepsy and the temporal lobes. A clinical, electroencephalographic and neuropathological study of the brain in epilepsy, with particular reference to the temporal lobes. *Brain* 89:499–530.

Meier R, Häussler U, Aertsen A, Deransart C, Depaulis A, Egert U. (2007) Short-term changes in bilateral hippocampal coherence precede epileptiform events. *Neuroimage* 38:138–149.

Nadel L, Hardt O. (2004) The spatial brain. *Neuropsychology* 18:473–476.

O'Keefe J, Recce ML. (1993) Phase relationship between hippocampal place units and the EEG theta rhythm. *Hippocampus* 3:317–330.

Riban V, Bouilleret V, Pham-Lê T, Fritschy JM, Marescaux C, Depaulis A. (2002) Evolution of hippocampal epileptic activity during the development of hippocampal sclerosis in a mouse model of temporal lobe epilepsy. *Neuroscience* 112:101–111.

Ryvlin P, Kahane P. (2005) The hidden causes of surgery-resistant temporal lobe epilepsy: extratemporal or temporal plus? *Curr Opin Neurol* 18:125–127.

Strogatz HS. (2000) *Nonlinear dynamics and chaos*. Westwood Press, Boulder, CO.

Sutula T, Cascino G, Cavazos J, Parada I, Ramirez L. (1989) Mossy fiber synaptic reorganization in the epileptic human temporal lobe. *Ann Neurol* 26:321–330.

Tang F, Loke W. (2009) Cyto-, axo- and dendro-architectonic changes of neurons in the limbic system in the mouse pilocarpine model of temporal lobe epilepsy. *Epilepsy Res* 89:43–51.

Tolner EA, Frahm C, Metzger R, Gorter JA, Witte OW, Lopes da Silva FH, Heinemann U. (2007) Synaptic responses in superficial layers of medial entorhinal cortex from rats with kainate-induced epilepsy. *Neurobiol Dis* 26:419–438.

Varga C, Lee SY, Soltesz I. (2010) Target-selective GABAergic control of entorhinal cortex output. *Nat Neurosci* 13:822–824.

Wilson HR, Cowan JD. (1972) Excitatory and inhibitory interactions in localized populations of model neurons. *Biophys J* 12:1–24.

Wozny C, Gabriel S, Jandova K, Schulze K, Heinemann U, Behr J. (2005) Entorhinal cortex entrains epileptiform activity in CA1 in pilocarpine-treated rats. *Neurobiol Dis* 19:451–460.

Yilmazer-Hanke DM, Wolf HK, Schramm J, Elger CE, Wiestler OD, Blümcke I. (2000) Subregional pathology of the amygdala complex and entorhinal region in surgical specimens from patients with pharmacoresistant temporal lobe epilepsy. *J Neuropathol Exp Neurol* 59:907–920.

Zahn RK, Tolner EA, Derst C, Gruber C, Veh RW, Heinemann U. (2008) Reduced ictogenic potential of 4-aminopyridine in the perirhinal and entorhinal cortex of kainate-treated chronic epileptic rats. *Neurobiol Dis* 29:186–200.

Supporting Information

Additional Supporting Information may be found in the online version of this article:

Figure S1. Raw and filtered traces show a shift in the theta band in KA activity as compared to control.

Figure S2. No distinct lag after shuffling of cutouts confirms the stability of Δt_{peak}.

Figure S3. Δt_{peak} values are stable across weeks in both groups.

Figure S4. Area CA1 appears synchronized with the DG in KA mice.

Figure S5. Block diagram of the Jansen model of coupled neuronal populations, examples, and power spectral density of the simulated signals.

Table S1. Physiologic interpretation and values of model parameters.

Supporting Methods. Detailed description of the computational model.

Please note: Wiley-Blackwell is not responsible for the content or functionality of any supporting information supplied by the authors. Any queries (other than missing material) should be directed to the corresponding author for the article.